

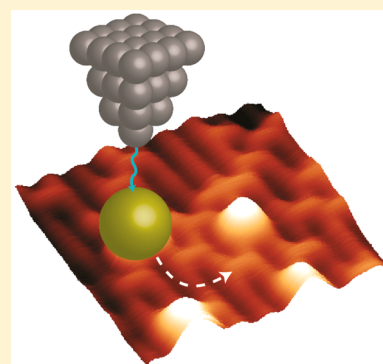
# Direct Visualization of Au Atoms Bound to TiO<sub>2</sub>(110) O-Vacancies

Andrew Mellor,<sup>†</sup> David Humphrey,<sup>†</sup> Chi M. Yim,<sup>†</sup> Chi L. Pang,<sup>†</sup> Hicham Idriss,<sup>†,‡</sup>  
and Geoff Thornton<sup>\*,†</sup>

<sup>†</sup>Department of Chemistry and London Centre for Nanotechnology, University College London, 20 Gordon Street, London WC1H 0AJ, United Kingdom

<sup>‡</sup>Fundamental Catalysis, SABIC-CRI at KAUST, Thuwal, Saudi Arabia

**ABSTRACT:** Au nanoparticles supported on reducible metal oxide surfaces are known to be active catalysts for a number of reactions including CO oxidation and hydrogen production. The exact choice of a metal oxide support has been shown to have a marked impact on activity, suggesting that interactions between Au and the support play a key role in catalysis. For TiO<sub>2</sub>, a model substrate for Au catalysis, it had been thought that bridging oxygen vacancies are involved in binding Au atoms to the (110) surface based on indirect evidence. However, a recent scanning transmission electron microscopy study of single Pt atoms on TiO<sub>2</sub>(110) suggests that subsurface vacancies are more important. To clarify the role of bridging or subsurface vacancies we employ scanning tunneling microscopy to determine the bonding site of single Au atoms on TiO<sub>2</sub>(110). Using in situ deposition as well as a manipulation method, we provide definitive evidence that the bonding site is atop surface oxygen vacancies.



## INTRODUCTION

The nature of the interaction of metal nanoparticles and their metal oxide supports remains a key area of research in catalysis.<sup>1–9</sup> In particular, gold nanoparticles supported on TiO<sub>2</sub> have received considerable attention<sup>2</sup> following the discovery that they are an effective low-temperature oxidation catalyst.<sup>3</sup> As a model catalyst, Au adsorption on rutile TiO<sub>2</sub>(110) has been extensively studied because this substrate is the most well-characterized metal oxide substrate.<sup>2,4–9</sup> When reduced, TiO<sub>2</sub> (110) contains point defects in the form of oxygen vacancies (O<sub>b</sub>-vacs) as well as Ti interstitial atoms in the bulk.<sup>5</sup> O<sub>b</sub>-vacs, in particular, are a widely studied aspect of TiO<sub>2</sub> fundamental catalysis because they are reactive sites on the surface and in many cases they act as bonding sites for surface adsorbates.<sup>5</sup>

A key feature of the Au/TiO<sub>2</sub> system that remains controversial is the bonding site of individual Au atoms on the surface (Au<sub>1</sub>). This is potentially important in connection to single atom catalysis, which has been demonstrated for a number of systems,<sup>10</sup> most recently for Au atoms on carbon.<sup>11</sup> On TiO<sub>2</sub>(110), Au<sub>1</sub> has been shown to be stable up to at least 600 K.<sup>6</sup> After soft landing Au<sup>+</sup>, Tong et al.<sup>6</sup> observed bonding of Au atoms to the bridging oxygen row using scanning tunneling microscopy (STM) and assigned the adsorption site to a bridging O<sub>b</sub>-vac. On cooling to 300 K they observed a reversible shift of adsorption site to the Ti row, assigning the adsorption site as atop a five-fold coordinated Ti site (Ti<sub>5c</sub>). This was interpreted as a displacement of Au<sub>1</sub> by interaction with adventitiously coadsorbed water at the lower temperature.<sup>6</sup> This is in line with previous spectroscopic work<sup>7</sup> and STM measurements.<sup>8</sup>

Although the STM results referenced above clearly observe Au<sub>1</sub> associated with the bridging O row, there is no direct evidence of bonding to O<sub>b</sub>-vac. On the contrary, several density functional theory (DFT) calculations suggest that O<sub>b</sub>-vac is the preferred site.<sup>8,9</sup> More recent results have challenged the assignment of O<sub>b</sub>-vac to the binding site of noble metals. In particular, aberration-corrected scanning transmission electron microscopy (STEM) has been used to image Pt<sub>1</sub> on TiO<sub>2</sub>(110). In their paper, the authors conclude that Pt<sub>1</sub> occupies in-plane O vacancies.<sup>12</sup> Theory predicts that the lowest energy site of Pt<sub>1</sub> atoms on reduced TiO<sub>2</sub>(110) is the same as for Au<sub>1</sub>, that is O<sub>b</sub>-vac.<sup>13</sup> Hence the implication of the STEM work is that Au<sub>1</sub> will also occupy in-plane O vacancies. If this was correct, then the discrepancy between DFT and experiment could arise from a dominance of kinetic effects. This has recently been demonstrated for a related system, Au-CeO<sub>2</sub>(111), where kinetic effects prevent the occupation of oxygen vacancies by Au<sub>1</sub>.<sup>14</sup> Here we demonstrate that this is not the case for Au<sub>1</sub> on a reduced rutile TiO<sub>2</sub>(110) surface (*r*-TiO<sub>2</sub>). We present direct evidence that single Au atoms bind at O<sub>b</sub>-vacs through a comparison of STM images of the same area on the surface before and after dosing Au<sub>1</sub>. We have also employed a method to selectively displace Au atoms using voltage pulses from an STM tip, thereby exposing the underlying O<sub>b</sub>-vac.

## EXPERIMENTAL METHODS

STM measurements employed two UHV Omicron instruments. One is a low-temperature bath cryostat machine (LT-

Received: September 27, 2017

Revised: October 17, 2017

Published: October 18, 2017

STM) operated at 78 K with a base pressure of  $3 \times 10^{-11}$  mbar. The second is a variable temperature microscope (VT-STM) operated at 300 K with a base pressure  $5 \times 10^{-11}$  mbar. A rutile  $\text{TiO}_2$  (110) ( $1 \times 1$ ) single-crystal (MaTeck) sample was prepared by successive cycles of argon ion sputtering and annealing to 1000 K. The sample cleanliness and long-range order were confirmed using X-ray photoelectron spectroscopy (XPS) or Auger electron spectroscopy (AES) and low-energy electron diffraction (LEED), respectively. Surfaces prepared in this manner typically have a coverage of  $\sim 5\%$  ML of  $\text{O}_b$ -vac (where 1 monolayer is the number of surface unit cells).

Au was deposited in situ onto an as-prepared  $\text{TiO}_2$ (110) surface present in the sample stage of the VT-STM at room temperature. Deposition was performed using a line-of-sight electron beam evaporator (Omicron EFM). The STM tip was retracted prior to deposition. In the LT-STM, Au was deposited onto as-prepared  $\text{TiO}_2$  (110) at room temperature using a Au rod wrapped around a tungsten filament, which was resistively heated to induce Au sublimation. The presence of Au on the  $\text{TiO}_2$  substrate was confirmed using XPS. In both systems, STM measurements were carried out in constant current mode using an electrochemically etched W tip conditioned by degassing at 500 K and voltage pulses in STM. There were no significant differences in Au coverage or dispersion seen in STM images recorded at 78 and 300 K.

## RESULTS AND DISCUSSION

Figure 1a shows an STM image of the as-prepared  $\text{TiO}_2$  (110) surface recorded after deposition of 0.08 monolayer (ML) of

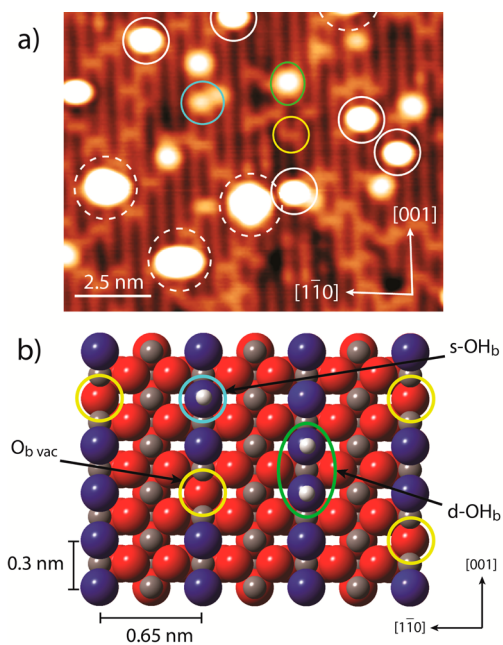


**Figure 1.** (a) STM image ( $V_S = +1.3$  V,  $I_T = 50$  pA) of  $r\text{-TiO}_2$  (110) at 78 K after deposition of 0.08 ML of Au at room temperature. The yellow solid circle marks an  $\text{O}_b$ -vac, whereas a blue circle and green ellipse mark single and paired hydroxyls ( $\text{OH}_b$ ), respectively. White solid and dashed circles mark  $\text{Au}_1$  and  $\text{Au}_3$  species, respectively. (b) On-top view structural model of  $\text{TiO}_2$ (110) illustrating  $\text{O}_b$ -vac and single (s-) and double (d-) OH groups. These are highlighted in the same colored circles as used in panel a. Ti atoms are depicted in brown, with O atoms in red and blue, the latter representing bridging  $\text{O}_b$  atoms.

Au. Au coverage was determined by measuring the average density of Au atoms on the surface via STM and dividing by the density of a single (111) layer of bulk gold, that is,  $1 \text{ ML} = 1.387 \times 10^{15} \text{ Au atoms}\cdot\text{cm}^{-2}$ .

In STM, the  $\text{TiO}_2$  (110) surface is characterized by bright rows of five-fold coordinated  $\text{Ti}^{4+}$  ( $\text{Ti}_{5c}$ ) and dark rows of two-fold bridging  $\text{O}^{2-}$  ( $\text{O}_b$ ) running along the [001] direction.<sup>5</sup> Five distinct types of features appear evenly distributed over the surface. The three smallest features are all centered over the  $\text{O}_b$  rows. The first appears as a small horizontal line (yellow circle), whereas the two larger features are more circular (blue circle and green ellipse). Such features are well described in the literature and are attributed to  $\text{O}_b$ -vac and  $\text{OH}_b$ , respectively.<sup>5</sup> A model showing these features is shown in Figure 1b. The two remaining unidentified features in Figure 1a are not typical of STM images from  $r\text{-TiO}_2$  (110) and can be attributed to deposited Au species. The first (highlighted as white solid circles in Figure 1a) appears centered over the  $\text{O}_b$  rows on the surface with an average height of  $193 \pm 60$  pm. The second (highlighted as white dashed circles in Figure 1a) is larger, spanning multiple  $\text{O}_b$  rows in the [110] direction with an average height of  $233 \pm 10$  pm. The larger Au species are found centered over either  $\text{O}_b$  or  $\text{Ti}_{5c}$  rows. Using STM in conjunction with DFT calculations, Matthey et al. identified the smallest Au species present on an Au-deposited  $r\text{-TiO}_2$  (110) to be  $\text{Au}_1$ .<sup>8</sup> The second smallest species they assign as Au trimers ( $\text{Au}_3$ ) that may adsorb in one of two geometries centered either over  $\text{O}_b$  or  $\text{Ti}_{5c}$  rows.<sup>8</sup> By direct comparison of our data with the previous work,<sup>8</sup> the smallest Au species observed in Figure 1a are assigned as  $\text{Au}_1$  and the larger ones to  $\text{Au}_3$ .

To unambiguously identify the binding site of  $\text{Au}_1$ , we performed in situ deposition of Au and imaged the same region of the  $r\text{-TiO}_2$  surface before and after deposition. This was achieved by collecting an STM image of  $r\text{-TiO}_2$  in an Omicron VT-STM instrument. The STM tip was then retracted and Au was deposited onto the imaged region using an in situ electron-beam evaporator that points to the STM stage. After deposition, the STM tip was reapproached to exactly the same position. Both the Au deposition and STM measurements were carried out at 300 K. As shown in Figure 2, after

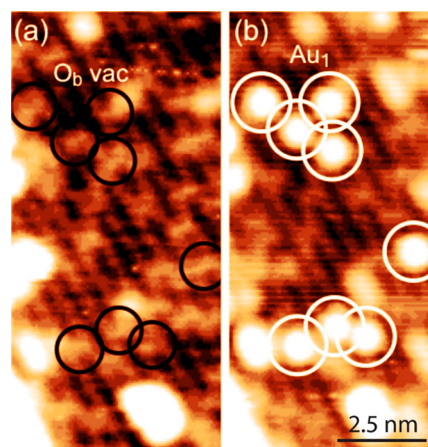


**Figure 2.** Room-temperature STM images ( $V_S = +1.3$  V,  $I_T = 20$  pA) of  $r\text{-TiO}_2$ (110) recorded (a) before and (b) after in situ deposition of  $<1\%$  ML Au at room temperature. Circles mark the  $\text{O}_b$ -vacs on  $r\text{-TiO}_2$  that are filled by  $\text{Au}_1$  after deposition. The bright (Ti) rows run in the [001] direction.

deposition some  $O_b$ -vacs that were on the  $r$ - $TiO_2$  are now filled by individual Au atoms (marked by circles in Figure 2a,b). Similar entities appear centered over  $Ti_{5c}$  rows but are much less frequent (<10%).

In addition, low-temperature measurements were also performed using an Omicron LT-STM system. At 78 K no  $Ti_{5c}$ -centered Au species were observed at all. On this basis, we conclude that  $O_b$ -vacs are the most stable binding sites for  $Au_1$  on the  $r$ - $TiO_2$  surface.

To provide further evidence that  $Au_1$  binds to  $O_b$ -vacs, STM tip pulsing was used to laterally manipulate  $Au_1$  on  $r$ - $TiO_2$ . STM tip-induced manipulation has been widely employed to form nanostructures on planar surfaces, and this field is reviewed in ref 15. To ensure stability and reproducibility, pulsing was performed at 78 K. Figure 3 shows atomically

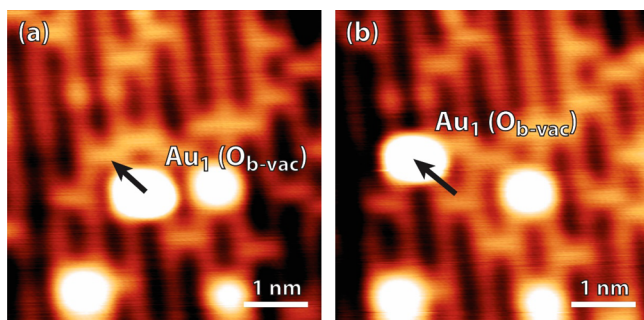


**Figure 3.** STM images ( $V_S = +1.2$  V,  $I_T = 10$  pA) of  $Au_1$  on  $r$ - $TiO_2(110)$  at 78 K showing its displacement from (a) one  $O_b$ -vac to (b) another  $O_b$ -vac site, induced by a 100 ms tip pulse over the  $Au_1$  species at a sample bias of  $-2$  V. Arrows indicate the directions of  $Au_1$  displacement. Three spectator adsorbates are present in the images, namely, a single and two double  $OH_b$  groups. The bright (Ti) rows run in the  $[001]$  direction.

resolved STM images of  $Au_1$  on  $r$ - $TiO_2(110)$  taken before (Figure 3a) and after (Figure 3b) application of a 100 ms tip pulse over the  $Au_1$  species at a sample bias of  $-2$  V.

By tracking its position before and after pulsing, the  $Au_1$  appears to move from its original site into an  $O_b$ -vac site on an adjacent  $O_b$  row ( $Au_{1-ovac}$ ). On inspection of the image in Figure 3b, the original position of the  $Au_1$ , which is now uncovered, is identified as an  $O_b$ -vac. To eliminate the possibility that this  $O_b$ -vac was generated as a consequence of the applied tip pulse, further tip pulses were performed over bare  $O_b$  rows using the same parameters. No  $O_b$ -vacs could be created by pulsing the bare  $r$ - $TiO_2(110)$ . Minato et al. have shown that it is possible to desorb  $O_b$  atoms using  $-2$  V tip pulses; however, in their work they use a pulse duration of 1 s compared with the 100 ms pulses applied here.<sup>16</sup> Hence the  $Au_1$  manipulation experiment also points to bonding with  $O_b$ -vac.

In addition to movement from one  $O_b$ -vac to another,  $Au_1$  could be manipulated from an  $O_b$ -vac onto a  $Ti_{5c}$  site ( $Au_{1-Ti}$ ) following application of a tip pulse (see Figure 4). The formation of these  $Au_{1-Ti}$  species was observed in a minority of movement events. After several STM scans ( $\sim 20$  min) the  $Au_{1-Ti}$  were seen to spontaneously move onto nearby  $O_b$ -vac sites becoming  $Au_{1-ovac}$ . After moving from  $Au_{1-Ti}$  to  $Au_{1-ovac}$  no subsequent changes were observed.

This supports the view that  $Au_1$  binds more strongly to  $O_b$ -vacs than to  $Ti_{5c}$  sites.<sup>8,9</sup> In this case, the observed  $Au_{1-Ti}$

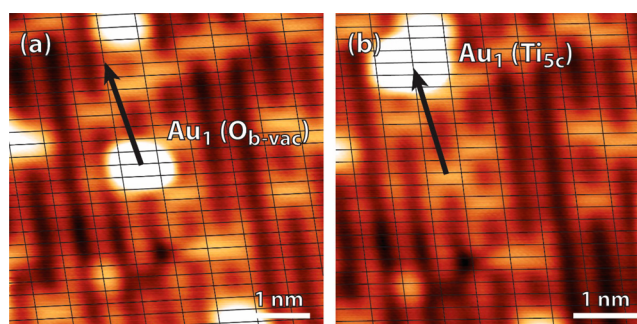


**Figure 4.** (a) STM images ( $V_S = +1.2$  V,  $I_T = 10$  pA) of  $Au_1$  on  $r$ - $TiO_2(110)$  at 78 K before (a) and after (b) STM tip-induced displacement of  $Au_1$  to a  $Ti_{5c}$  row induced by a  $-2$  V, 100 ms tip pulse centered above  $Au_1$ . The  $TiO_2(110)$  surface lattice has been overlaid on the image, where intersections in the grid indicate  $Ti_{5c}$  positions. Arrows indicate the movement of  $Au_1$  from an  $O_b$ -vac to a  $Ti_{5c}$  site. The bright (Ti) rows run in the  $[001]$  direction.

complex is likely to have been stabilized by the cryogenic conditions used (78 K).

To determine the underlying mechanism of  $Au_1$  displacement, a detailed statistical analysis of pulsing events was performed. This follows a methodology used previously to investigate tip-induced H desorption from  $Si(100)-2\times 1:H^{17}$  and  $TiO_2(110)-OH^{18}$ . During a tip pulsing experiment the STM tip is first centered over an  $Au_1$  species. By monitoring the tunneling current ( $I_T$ ) for the duration of each pulse, a plot of  $I_T(t)$  is created (Figure 5 inset). For each pulse an  $I_T$  set point

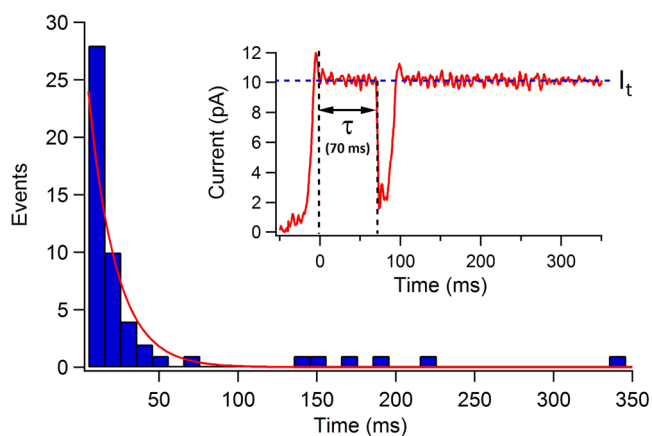


**Figure 5.** Histogram showing the distribution of  $Au_1$  displacement times for tip pulses of  $V_S = -1.8$  V and  $I = 10$  pA. The red line represents an exponential fit to the distribution of statistically independent events. The inset is an example of an individual  $I(t)$  trace used to compile the histogram where  $I_t$  is the set point of the pulse (10 pA) and  $\tau$  is the pulse duration prior to Au displacement.

is reached and held constant by the feedback loop of the STM. During manipulation, a peak in the  $I_T(t)$  plot can be seen. This peak corresponds to the sudden displacement of the  $Au_1$  beneath the tip. The increase in tip-sample distance caused by the now absent  $Au_1$  decreases  $I_T$  sharply before the feedback loop corrects for the change by bringing  $I_T$  back to the initial set point. The pulse duration required to induce movement can be determined from the position of the excursion in  $I_T$ . This process was repeated multiple times ( $\sim 60$ ) for each set of pulsing parameters used in this work. After plotting the resulting data in histogram form, an exponential decay was fit to

the data to yield the average value of  $\tau$  for each pulsing parameter, an example being shown in Figure 5. For each plotted histogram, bin widths were varied, within a reasonable range, such that the resulting change in  $\tau$  could be factored into the error of each average value determined.

To confirm that the measured distribution of Au<sub>1</sub> displacement times does indeed follow an exponential decay, a semilog plot of  $\ln N(t)$  was created for each data set (Figure 6).

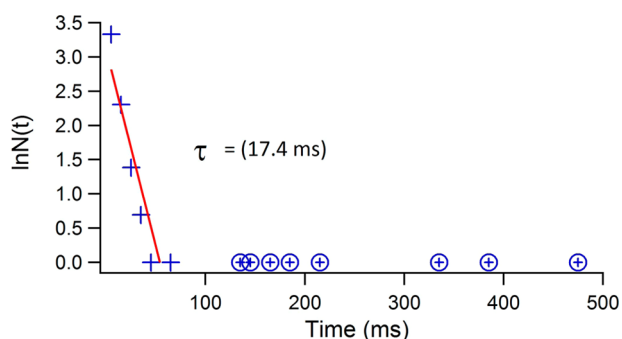


**Figure 6.** Plot of  $\ln N(t)$  versus time for the data shown in Figure 5. The red line shows a linear fit to the data. The last eight points of the plot have been attributed to random noise and are omitted from the fitting. From the slope of the linear fit,  $\tau$  was determined to be 17.4 ms. The fitting from this plot was used to refine the exponential fitting to the histogram shown in Figure 5 and hence the value of  $\tau$ .

The displacement yield (events per electron),  $Y$ , was determined using the average value of  $\tau$  measured for each pulsing parameter.  $Y$  values were calculated for a range of pulsing currents and voltages and were plotted as a function of  $I_T$ . The relationship between  $Y$  and  $I_T$  was then used to determine the displacement reaction order, that is, the number of principal electrons involved in the dissociation of a single Au<sub>1</sub> from an O<sub>b</sub> vac (Figure 7). Because for an  $n$ -electron

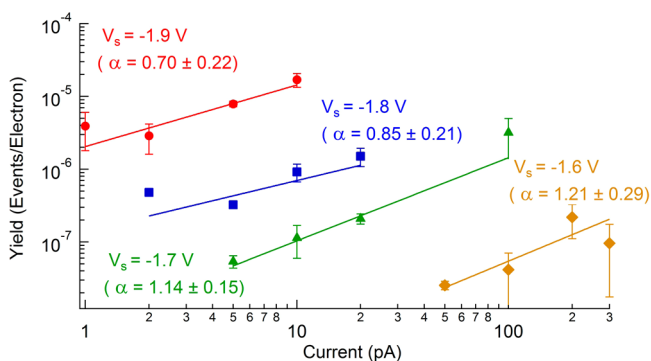


**Figure 7.** Double-logarithmic plot of displacement yield,  $Y$ , as a function of tunneling current,  $I_T$ . Solid circles, squares, triangles, and rhombi represent the measured yields of Au<sub>1</sub> displacements at different pulse voltages (labeled). Lines show power-law fits to the experimental data, with exponents ( $\alpha$ ) given for each pulse voltage.

process  $Y \propto I_T^{(n-1)}$ ,<sup>18</sup> the gradients observed in Figure 7, which are approximately unity, indicate a two-electron vibrational ladder-climbing process. Such a mechanism is typical for adsorbates on semiconductors<sup>15</sup> and has been proposed previously for STM tip-induced dissociation of H from TiO<sub>2</sub>(110)-OH.<sup>18</sup>

## CONCLUSIONS

The direct evidence provided here for bonding of gold atoms to bridging oxygen vacancies on TiO<sub>2</sub>(110) is clearly in accord with the predictions of DFT calculations.<sup>8,9</sup> There is, however, a marked disagreement between this work and the conclusions of a scanning transmission electron microscopy study of platinum atoms on TiO<sub>2</sub>(110).<sup>12</sup> In this previous work, bond sites atop subsurface vacancies were proposed, with no observed bonding to bridging oxygen vacancies. A likely cause of this difference is that the surface in the previous work was hydroxylated, a state that is known to promote occupation of Ti<sub>5c</sub> sites.<sup>6,8</sup> Hence, our result removes an important discrepancy in the literature between theory and experiment and reinstates the importance of bridging oxygen vacancies in the catalytically related chemistry of TiO<sub>2</sub>.

## AUTHOR INFORMATION

### Corresponding Author

\*E-mail: g.thornton@ucl.ac.uk.

### ORCID

Geoff Thornton: 0000-0002-1616-5606

### Notes

The authors declare no competing financial interest.

## ACKNOWLEDGMENTS

C.M.Y., C.L.P., and G.T. were supported by the European Research Council Advanced Grant ENERGYSURF and European Cooperation in Science and Technology Action CM1104. G.T. was also supported by the Alexander von Humboldt Stiftung and by a Royal Society Wolfson Research Merit Award. A.M. and D.H. were supported by EPSRC (UK) (EP/G036675/1, GR/R45680/01). A.M. was also supported by SABIC UK.

## REFERENCES

- (1) Bell, A. T. The Impact of Nanoscience on Heterogeneous Catalysis. *Science* **2003**, *299*, 1688–1691.
- (2) Panayotov, D. A.; Morris, J. R. Surface Chemistry of Au/TiO<sub>2</sub>: Thermally and Photolytically Activated Reactions. *Surf. Sci. Rep.* **2016**, *71*, 77–271.
- (3) Haruta, M. Size- and Support-Dependency in the Catalysis of Gold. *Catal. Today* **1997**, *36*, 153–166.
- (4) Valden, M.; Lai, K.; Luo, Q.; Guo, Q.; Goodman, D. W. Onset of Catalytic Activity of Gold Clusters on Titania with the Appearance of Nonmetallic Properties. *Science* **1998**, *281*, 1647–1650.
- (5) Pang, C. L.; Lindsay, R.; Thornton, G. Structure of Clean and Adsorbate-Covered Single-Crystal Rutile TiO<sub>2</sub> Surfaces. *Chem. Rev.* **2013**, *113*, 3887–3948.
- (6) Tong, X.; Benz, L.; Chrétien, S.; Metiu, H.; Bowers, M. T.; Buratto, S. K. Direct Visualization of Water-Induced Relocation of Au Atoms from Oxygen Vacancies on a TiO<sub>2</sub>(110) Surface. *J. Phys. Chem. C* **2010**, *114*, 3987–3990.
- (7) Lee, S.; Fan, C.; Wu, T.; Anderson, S. L. CO Oxidation on Au<sub>n</sub>/TiO<sub>2</sub> Catalysts Produced by Size-Selected Cluster Deposition. *J. Am. Chem. Soc.* **2004**, *126*, 5682–5683.
- (8) Matthey, D.; Wang, J. G.; Wendt, S.; Matthiesen, J.; Schaub, R.; Laegsgaard, E.; Hammer, B.; Besenbacher, F. Enhanced Bonding of Gold Nanoparticles on Oxidized TiO<sub>2</sub>(110). *Science* **2007**, *315*, 1692–1696.
- (9) Chrétien, S.; Metiu, H. J. Density Functional Study of the Interaction Between Small Au Clusters, Au<sub>n</sub> (n = 1–7) and the Rutile TiO<sub>2</sub> Surface. II. Adsorption on a Partially Reduced Surface. *J. Chem. Phys.* **2007**, *127*, 244708.

(10) Thomas, J. M. Catalysis: Tens of Thousands of Atoms Replaced by One. *Nature* **2015**, *525*, 325–326.

(11) Malta, G.; Kondrat, S. A.; Freakley, S. J.; Davies, C. J.; Lu, L.; Dawson, S.; Thetford, A.; Gibson, E. K.; Morgan, D. J.; Jones, et al. Identification of Single-Site Gold Catalysis in Acetylene Hydrochlorination. *Science* **2017**, *355*, 1399–1403.

(12) Chang, T.-Y.; Tanaka, Y.; Ishikawa, R.; Toyoura, K.; Matsunaga, K.; Ikuhara, Y.; Shibata, N. Direct Imaging of Pt Single Atoms Adsorbed on TiO<sub>2</sub> (110). *Nano Lett.* **2014**, *14*, 134–138.

(13) Çelik, V.; Ünal, H.; Mete, E.; Ellialtıođlu, Ş. Theoretical Analysis of Small Pt Particles on Rutile TiO<sub>2</sub>(110) Surfaces. *Phys. Rev. B: Condens. Matter Mater. Phys.* **2010**, *82*, 205113.

(14) Lustemberg, P. G.; Pan, Y.; Shaw, B.-J.; Grinter, D.; Pang, C.; Thornton, G.; Pérez, R.; Ganduglia-Pirovano, M. V.; Nilius, N. Diffusion Barriers Block Defect Occupation on Reduced CeO<sub>2</sub>(111). *Phys. Rev. Lett.* **2016**, *116*, 236101.

(15) Morgenstern, K.; Lorente, N.; Rieder, K.-H. Controlled Manipulation of Single Atoms and Small Molecules Using the Scanning Tunneling Microscope. *Phys. Status Solidi B* **2013**, *250*, 1671–1751.

(16) Minato, T.; Kawai, M.; Kim, Y. Creation of Single Oxygen Vacancy on Titanium Dioxide Surface. *J. Mater. Res.* **2012**, *27*, 2237–2240.

(17) Soukiassian, L.; Mayne, A. J.; Carbone, M.; Dujardin, G. Atomic-Scale Desorption of H Atoms from the Si(100)-2 × 1:H Surface: Inelastic Electron Interactions. *Phys. Rev. B: Condens. Matter Mater. Phys.* **2003**, *68*, 035303.

(18) Acharya, D. P.; Ciobanu, C. V.; Camillone, N., III; Sutter, P. Mechanism of Electron-Induced Hydrogen Desorption from Hydroxylated Rutile TiO<sub>2</sub> (110). *J. Phys. Chem. C* **2010**, *114*, 21510–21515.